The Meteoritical Society

Meteoritics & Planetary Science 44, Nr 8, 1095–1105 (2009)
Abstract available online at http://meteoritics.org

Atmospheric erosion induced by oblique impacts

V. SHUVALOV

Institute of Geosphere Dynamics, 38 Leninsky prosp. Bld.1, 119334 Moscow, Russia
*Corresponding author. E-mail: shuvalov@idg.chph.ras.ru

(Received 31 March 2009; revision accepted 27 May 2009)

Abstract–Previous investigations of impact-induced atmospheric erosion considered vertical impacts only. Numerical simulations of oblique impacts presented in this paper show that the loss of air strongly depends on trajectory inclination and it increases as the impact angle decreases. The results of numerical simulations over the wide range of impact parameters (projectile sizes from 1 to 30 km, impact velocities from 15 to 70 km/s, escape velocities from 5 to 11.2 km/s, projectile densities from 1 to 3.3 g/cm^3, normal atmospheric densities varying by three orders of magnitude) can be approximated by simple analytical formulae.

INTRODUCTION

The idea of planetary atmospheric erosion resulting from asteroid impacts was suggested by Cameron (1983). It is based on the assumption that a considerable mass of shock-heated and upward accelerated atmospheric air can reach velocities exceeding u_{esc} = 11.2 km/s (i.e., escape velocity for the Earth) and can be ejected to space. The first estimates of impact induced atmospheric erosion were obtained by using a simplified sector blow-off model (Vickery and Melosh 1990). This approximation uses the Zel'dovich and Raizer (1967) solution for expansion of a vapor plume and momentum balance between the expanding gas and the mass of the overlying atmosphere. The model predicts a cone-shaped escape region with the angle of taper depending on impact energy. The blow-off model was widely used to study the evolution of planetary atmospheres (see, e.g., Zahnle et al. 1990, 1992).

Later Newman et al. (1999), using a more sophisticated analytical model based on the solution of Kompaneets (1960) and a numerical model with simplified initial conditions, concluded that the mass of escaping air is significantly less (by a factor of about five for Chicxulub-scale impacts) than predicted by the blow-off model. In these simulations, the authors did not consider a real impact (penetration and excavation stages). Instead, they assumed that the initial vapor cloud had a pancake or pillbox shape with density approximating that of lithospheric material.

However, both models did not take into account the influence of atmospheric perturbations generated during the impactor flight through the atmosphere and the influence of the cratering process on air ejection. The significance of these factors was outlined by Vickery (1994) and Svetsov (1996). Detailed numerical simulations (Shuvalov and Artemieva 2000, 2002) taking into account both the projectile interaction with the atmosphere and the cratering process have shown that vertical impacts of both comets and asteroids with diameters exceeding 1 km could not considerably erode the Earth's atmosphere. The ratio of escaping mass to the impactor mass in vertical impacts is less than predicted by both blow-off and Newman's models. It does not exceed the value of 2–3%, which is significantly less than the mass of volatiles delivered by impactors (Chyba 1990) and released during the impact (Pierazzo et al. 1998).

Nemtchinov and Shuvalov (2003) and Svetsov (2007) have shown that vertical impacts of comets 100 to 300 m in diameter could provide strong erosion of the Earth's atmosphere. In such impacts, the ratio of escaping mass to the impactor mass reaches up to a few tens percent. Thus they could strongly influence the evolution of the atmosphere. However, the existence of such small comets and their number are still being questioned. At least, small comets are not considered to be a major type of Earth's impactors (Kuzmitcheva and Ivanov 2008).

Most previous papers considered atmospheric erosion after vertical impacts only. However, preliminary results (Shuvalov and Artemieva 2002) obtained in simulations with low resolution have shown that the escaping mass in oblique impacts could be much higher than in vertical ones. The aim of the present study is to calculate the loss of air in oblique impacts of large (1 to 30 km) asteroids and comets.

Table 1. Relative masses of escaping air, projectile and target material for different variants of asteroidal impacts D-V-A (D-projectile diameter (in km), V-impact velocity (km/s), A-impact angle), two values of escape velocity (11.2 and 5 km/s), and modern Earth's atmosphere. Angle-averaged escaping masses are shown in brackets in lines for 45 degree impact angles. The values of dimensionless erosional power for escape velocities 11.2 km/s ($\xi_{11.2}$) and 5 km/s (ξ_5) are given in the last column.

Variant	m_a/M (u_{esc} = 11.2)	m_a/M (u_{esc} = 5)	m_{pr}/M (u_{esc} = 11.2)	m_{pr}/M (u_{esc} = 5)	m_t/M (u_{esc} = 11.2)	m_t/M (u_{esc} = 5)	$\xi_{11.2}$ (ξ_5)
01-20-15	2e-5	0.04	0	0	0	3e-5	
01 20-30	1E-3	0.5	0	0.08	0	5e-3	
01-20-45	3E-4 (3e-4)	0.2 (0,2)	0 (0)	0.05 (0,03)	0 (0)	0.01 (7e-3)	5.1 (33)
01-20-60	1e-4	0.03	0	3e-3	0	0.01	
01-20-90	1e-5	7e-3	0	1.5e-4	0	2e-3	
03-20-15	0.02	1	4e-3	0.3	0	0.02	
03-20-30	0.08	0.4	0.2	0.3	0.02	0.4	
03-20-45	0.025 (0,029)	0.1 (0,25)	0.03 (0,04)	0.1 (0,2)	2e-3 (5e-3)	0.25 (0,2)	1.4e2 (9e2)
03-20-60	4e-3	0.05	1E-4	0.02	5E-3	0.18	
03-20-90	1e-4	8e-3	0	7e-4	0	2e-3	
10-20-15	0.15	0.3	0.3	0.4	0.03	0.09	
10 20-30	0.03	0.06	0.3	0.4	0.07	0.6	
10-20-45	0.01 (0,03)	0.025 (0,06)	0.04 (0,2)	0.15 (0,25)	0.03 (0,029)	0.3 (0,30)	5.1e3 (3.3e4)
10-20-60	5e-3	0.01	4e-3	0.02	6e-3	0.2	
10-20-90	2e-4	2e-3	1e-4	0.015	2e-4	0.02	
30-20-15	0.025	0.03	0.3	0.5	0.04	0.08	
30-20-30	6e-3	0.01	0.3	0.5	0.07	0.6	
30-20-45	2e-3 (5e-3)	5e-3 (0,01)	0.04 (0,1)	0.15 (0,25)	0.04 (0,04)	0.4 (0,3)	1.4e5 (9e5)
30-20-60	1e-3	0.01	4e-3	0.02	7e-3	0.2	
30-20-90	1e-3	0.01	2e-3	0.02	2e-4	0.02	
01-15-15	0	3e-3	0	0	0	0	
01-15-30	1e-5	0.02	0	1e-4	0	0	
01-15-45	2e-5 (1e-5)	0.04 (0,02)	0 (0)	0.04 (0,015)	0 (0)	0 (0)	1.9 (18)
01-15-60	2e-6	0.01	0	1e-4	0	0	
01-15-90	2e-6	1e-3	0	1e-4	0	0	
03-15-15	0	0.4	0	0.06	0	1.5e-3	
03-15-30	0.025	0.3	1e-3	0.25	0	0.15	
03-15-45	0.01 (0,01)	0.1 (0,16)	5e-4 (4e-4)	0.2 (0,15)	0 (0)	0.15 (0,1)	52 (4.8e2)
03-15-60	7E-4	0.05	0	0.02	0	0.05	
03-15-90	2e-4	0.01	0	2e-4	0	0	
10-15-15	0.03	0.4	6e-3	0.3	0	0.05	
10 15-30	0.02	0.05	0.2	0.3	0.02	0.2	
10-15-45	8e-3 (0,01)	0.02 (0,07)	0.06 (0,06)	0.2 (0,2)	0.04 (0,015)	0.4 (0,20)	1.9e3 (1.8e4)
10-15-60	3e-3	0.01	3e-3	0.02	5e-4	0.09	
10-15-90	2e-4	2e-3	0	2e-4	0	7e-3	
30-15-15	0.02	0.04	0.1	0.3	5e-3	0.05	
30-15-30	5e-3	5e-3	0.2	0.3	0.02	0.2	
30-15-45	2.5e-3 (4e-3)	4e-3 (0,07)	0.04 (0,07)	0.1 (0,2)	0.05 (0,02)	0.4 (0,2)	5.2e4 (4.8e5)
30-15-60	1.2E-3	3E-3	3E-3	0.02	3.4E-3	0.1	
30-15-90	2e-4	1e-3	0	2e-4	0	1e-2	

NUMERICAL MODEL

A 3D version of the SOVA multi-material hydrocode (Shuvalov 1999) was used to model the interaction of the impactor with the atmosphere and solid Earth. The SOVA is an Eulerian material response code with some Lagrangian features. It allows considering strong hydrodynamic flows with accurate description of the boundaries between different materials (e.g., vapor, air, solid impactor, etc.). The governing transport equations consist of conservation equations of mass, momentum, and energy, which are solved for gas/liquid/solid. In the first step, the Lagrangian equations are solved using a second-order difference scheme; in the second step, the data is reinterpolated (remapped) from the Lagrangian grid to the Eulerian grid with the second order accuracy.

The target was considered to consist of granite with density of 2.63 g/cm^3. The target strength was not taken into account because the high velocity part of the impact plume

Table 2. Relative masses of escaping air, projectile and target material for different variants of cometary impacts D-V-A (D-projectile diameter (in km), V-impact velocity (km/s), A-impact angle), two values of escape velocity (11.2 and 5 km/s), and modern atmosphere. Angle-averaged escaping masses are shown in brackets in lines for 45 degree impact angles. The values of dimensionless erosional power for escape velocities 11.2 km/s ($\xi_{11.2}$) and 5 km/s (ξ_5) are given in the last column.

Variant	m_a/M (u_{esc} = 11.2)	m_a/M (u_{esc} = 5)	m_{pr}/M (u_{esc} = 11.2)	m_{pr}/M (u_{esc} = 5)	m_t/M (u_{esc} = 11.2)	m_t/M (u_{esc} = 5)	$\xi_{11.2}$ (ξ_5)
01-30-15	0	0.03	0	0	0	0	
01-30-30	0	1	0	0.2	0	0.01	
01-30-45	0.02 (0.011)	0.7 (0.56)	0 (0.0054)	0.6 (0.41)	0 (0)	0.04 (0.026)	7.1 (38)
01-30-60	0.015	0.4	0	0.5	0	0.04	
01-30-90	0.01	0.05	0.08	0.5	0	0	
03-30-15	0.5	3	0.6	0.8	0.01	0.3	
03-30-30	0.3	1.5	0.5	0.8	4e-4	0.2	
03-30-45	0.2 (0.21)	0.7 (1.0)	0.4 (0.38)	0.9 (0.81)	0.02 (0.01)	0.4 (0.41)	19 (1.0e3)
03-30-60	0.08	0.4	0.2	0.7	0.006	0.6	
03-30-90	0.005	0.1	0.15	0.8	0	0.5	
10-30-15	0.15	0.3	0.45	0.65	0	0.01	
10-30-30	0.1	0.2	0.75	0.9	0.07	0.2	
10-30-45	0.06 (0.07)	0.15 (0.16)	0.5 (0.47)	0.9 (0.79)	0.15 (0.09)	0.5 (0.41)	7.1e3 (3.8e4)
10-30-60	0.03	0.1	0.3	0.7	0.09	0.65	
10-30-90	0.015	0.06	0.15	0.5	1.5e-3	0.4	
30-30 15	0.03	0.05	0.9	1	5e-3	0.07	
30-30-30	0.04	0.06	0.8	1	0.07	0.25	
30-30-45	0.008 (0.017)	0.015 (0.029)	0.5 (0.53)	0.8 (0.82)	0.15 (0.093)	0.8 (0.58)	1.9e5 (1.0e6)
30-30-60	7e-3	0.015	0.3	0.7	0.1	0.8	
30-30-90	1e-3	0.015	0.1	0.5	0.01	0.5	
01-50-15	0.02	4	0	0.2	0	0.01	
01-50-30	0.2	4	0.1	0.8	0.01	0.05	
01-50-45	0.2 (0,14)	3 (2,8)	0.4 (0,2)	0.8 (0,8)	3e-3 (9e-3)	0.8 (0,6)	22 (1.1e2)
01-50-60	0.1	1.6	0.3	0.9	0.02	1.2	
01-50-90	0.06	0.9	0.2	0.9	0.01	0.95	
03-50-15	1	3.5	0.8	0.9	0.02	0.4	
03-50-30	0.7	2	0.9	0.9	0.1	0.1	
03-50-45	0.4 (0,5)	0.9 (1,3)	0.8 (0,7)	0.9 (0,9)	0.3 (0,2)	1.8 (1,3)	5.8e2 (2.9e3)
03-50-60	0.2	0.6	0.6	0.9	0.3	1.9	
03-50-90	0.04	0.4	0.5	0.9	0.1	2	
10-50-15	0.25	0.5	0.9	0.9	0.05	0.4	
10-50-30	0.2	0.4	0.9	1	0.3	1	
10-50-45	0.1 (0,12)	0.16 (0,24)	0.8 (0,8)	1 (0,9)	0.5 (0,4)	1.8 (1,5)	2.2e4 (1.1e5)
10-50-60	0.05	0.1	0.6	0.9	0.5	1.9	
10-50-90	0.02	0.2	0.5	0.9	0.2	2	
30-50-15	0.03	0.05	0.9	0.9	0.08	0.4	
30-50-30	0.02	0.04	0.9	1	0.3	1	
30-50-45	0.01 (0,01)	0.03 (0,02)	0.8 (0,8)	1 (0,9)	0.5 (0,4)	2 (1,7)	5.8e5 (2.9e6)
30-50-60	5e-3	0.03	0.6	0.9	0.4	2	
30-50-90	3e-3	0.02	0.5	0.9	0.2	2	
01-70-15	0.15	10	0.04	0.4	0	0.15	
01-70-30	0.15	9	0.6	0.9	0.1	1.5	
01-70-45	0.8 (0.46)	6 (6.3)	0.8 (0.62)	1 (0.9)	0.2 (0.1)	3.5 (3.1)	43 (2.1e2)
01-70-60	0.5	4	0.6	1	0.05	5	
01-70-90	0.1	1.5	0.8	1	0.001	4	
03-70-15	3	6	0.7	0.8	0.2	0.8	
03-70-30	0.3	1.5	1	1	0.7	2.5	
03-70-45	0.6 (0.70)	1.5 (1.8)	1 (0.9)	1 (0.95)	1 (0.75)	1 (2.5)	1.2e3 (5.8e3)
03-70-60	0.3	0.8	1	1	0.8	5	
03-70-90	0.06	0.8	0.9	1	0.4	3	
10-70-15	0.4	0.9	1	1	0.3	0.8	

Table 2. *Continued.* Relative masses of escaping air, projectile and target material for different variants of cometary impacts D-V-A (D-projectile diameter (in km), V-impact velocity (km/s), A-impact angle), two values of escape velocity (11.2 and 5 km/s), and modern atmosphere. Angle-averaged escaping masses are shown in brackets in lines for 45 degree impact angles. The values of dimensionless erosional power for escape velocities 11.2 km/s ($\xi_{11.2}$) and 5 km/s (ξ_5) are given in the last column.

Variant	m_a/M (u_{esc} = 11.2)	m_a/M (u_{esc} = 5)	m_{pr}/M (u_{esc} = 11.2)	m_{pr}/M (u_{esc} = 5)	m_t/M (u_{esc} = 11.2)	m_t/M (u_{esc} = 5)	$\xi_{11.2}$ (ξ_5)
10-70-30	0.3	0.6	1	1	0.7	2	
10-70-45	0.1 (0.2)	0.25 (0.4)	1 (1)	1 (1)	1(0.8)	4 (3.7)	4.3e4 (2.1e5)
10-70-60	0.07	0.15	0.9	0.9	1	6	
10-70-90	0.04	0.15	0.9	1	0.6	4	
30-70-15	0.06	0.1	1	1	0.3	0.8	
30-70-30	0.05	0.1	1	1	0.5	2	
30-70-45	0.01 (0.025)	0.02 (0.049)	0.8 (0.9)	1 (0.98)	0.5 (0.60)	2 (2.5)	1.2e6 (5.8e6)
30-70-60	0.015	0.03	0.9	1	0.9	3	
30-70-90	4e-3	0.015	0.8	0.9	0.8	7	

(which is responsible for atmospheric erosion) is generated by ejection and expansion of strengthless melted and partially vaporized target and projectile materials. Numerical simulations were performed for cylindrical asteroids consisting of dunite with density of 3.32 g/cm^3 and comets consisting of water with density of 1 g/cm^3. The height of a cylinder of diameter D was defined from the condition that the cylinder's volume equals the volume of a sphere with the same diameter D. Impacts of stony bodies at velocities of 15 and 20 km/s and impacts of comets at velocities of 30, 50, and 70 km/s were considered.

Tables obtained with the ANEOS equation of state (Thomson and Lauson 1972) and input data from Pierazzo et al. (1997) were used to describe thermodynamical properties of granite and dunite. Tabular equation of state (Kosarev 2008) was used to describe thermodynamical properties of water.

Up to 100,000 tracer particles were regularly distributed in the atmosphere to determine the initial position of escaping air, i.e., the escape region. The tracers are passive massless particles that move through the mesh with the gas velocity, recording trajectories and current velocities of given material points.

In the simulations, the projectile impacts the target at angles 15, 30, 45, 60, and 90° (vertical) from the horizon. Each simulation starts with the projectile at an altitude of 6 D, where D is the projectile diameter. The initial cell sizes were D/40 (40 cells across projectile diameter). The cell size and the size of the computational region were doubled when the plume or the shock wave in the target material reached the grid boundary. The final vertical cell size h_z did not exceed 1.5 km, the horizontal cell sizes h_x and h_y did not exceed 6 km. The curvature of the Earth was taken into account for large ($D \geq 10$ km) projectiles.

Bilateral symmetry was used that allowing the modeling of only the positive half-space $y > 0$ originating from the impact plane (plane perpendicular to the target and passing through the trajectory). Numerical mesh consisted of 270 × 100 × 270 cells in x (horizontal in the plane of trajectory), y (horizontal perpendicular to the trajectory plane), and z (vertical) directions correspondingly.

The mass of escaping air m_a was determined as material flux through the surface z = 100 km:

$$m_a = \int f \rho_a u_z dx dy dt, \quad (1)$$

where ρ_a is air density, u and u_z are flow velocity and its vertical component, dt is time interval, $f = 1$ if $u > u_{esc}$ and $u_z > 0$, otherwise $f = 0$. The summation is over the surface z = 100 km. The mass of escaping target m_t and projectile m_{pr} materials were also determined in the same way.

NUMERICAL RESULTS

Numerical results for the modern Earth's atmosphere are summarized in Table 1 for asteroidal impacts and Table 2 for cometary impacts. The first conclusion is that the impact angle strongly (in some cases by orders of magnitude) influences atmospheric erosion. Figure 1 illustrates the main reasons for this influence. Projectile penetration into the planetary atmosphere results in formation of a wake, i.e., a rarefied hot channel with density 1–2 orders of magnitude lower than the ambient air density. In vertical impacts, an impact plume expands preferably along the wake, because the fastest (and with lower density) part of the plume undergoes a considerable atmospheric drag outside the wake. The wake in this case works like an empty tube through which the hot rarefied vapor moves to high altitudes. The shock wave generated by the plume also propagates preferably along the wake and strongly accelerates the small mass of air filling the wake and surrounding the wake. In oblique impacts, the plume develops outside the wake (in downrange direction), expands more isotropically (see Fig. 1), and involves in the motion (and accelerates) a greater mass of atmospheric air. This effect is more important for small (<10 km) projectiles producing plumes, which are more affected by atmospheric

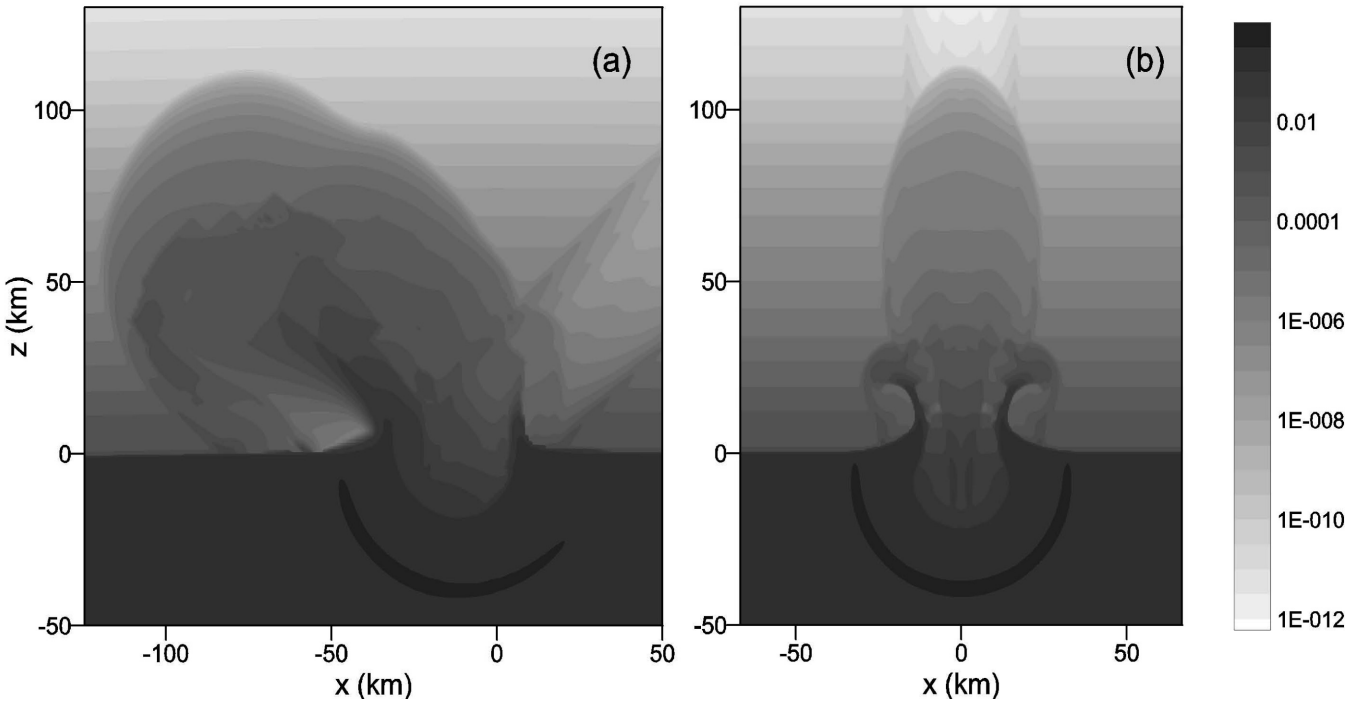

Fig. 1. Comparison between a 45° oblique impact (a) and a vertical (b) impact of an asteroid 10 km in diameter. Density distributions are shown. Impact plume moves within the wake in a vertical impact, whereas it expands outside the wake in an oblique impact.

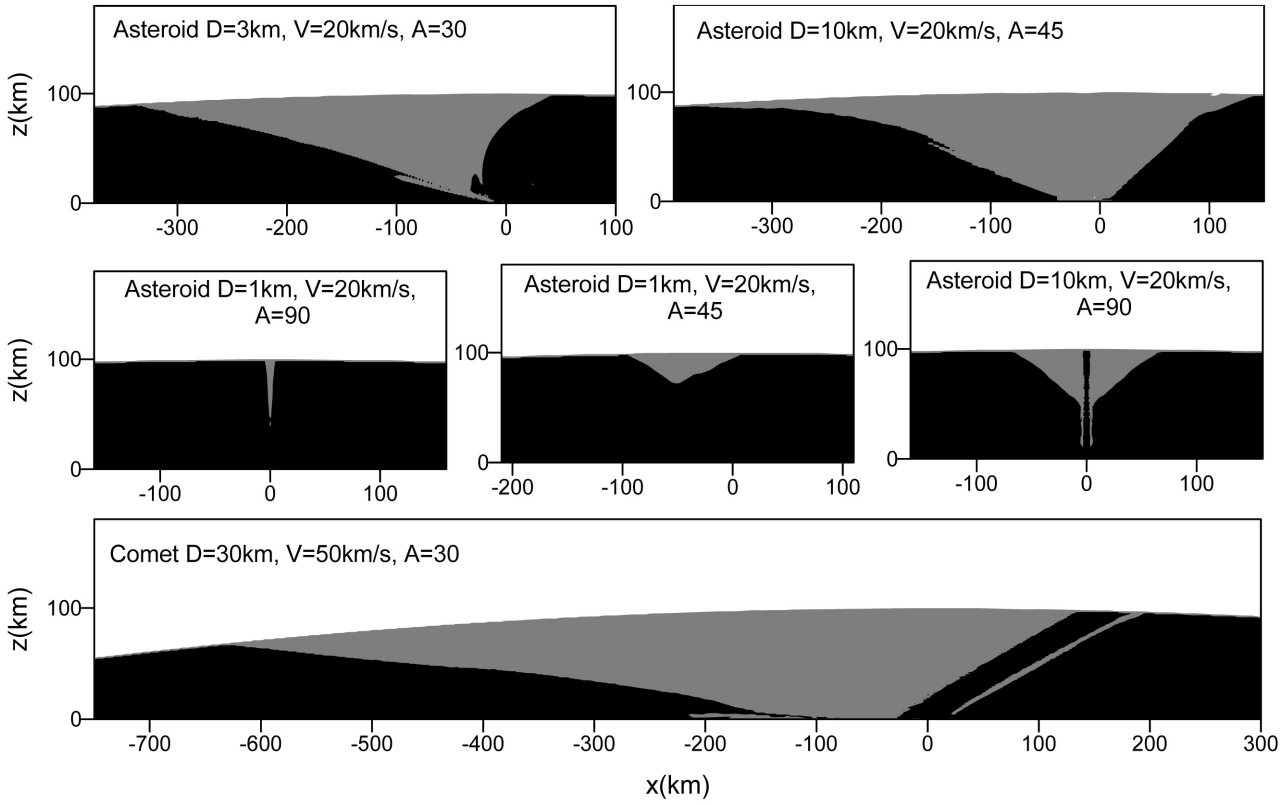

Fig. 2. Some typical escape regions. Gray shading shows initial position of escaping air (accelerated above 11.2 km/c), black shading shows initial position of nonescaping air. Only a 100 km atmospheric layer is shown.

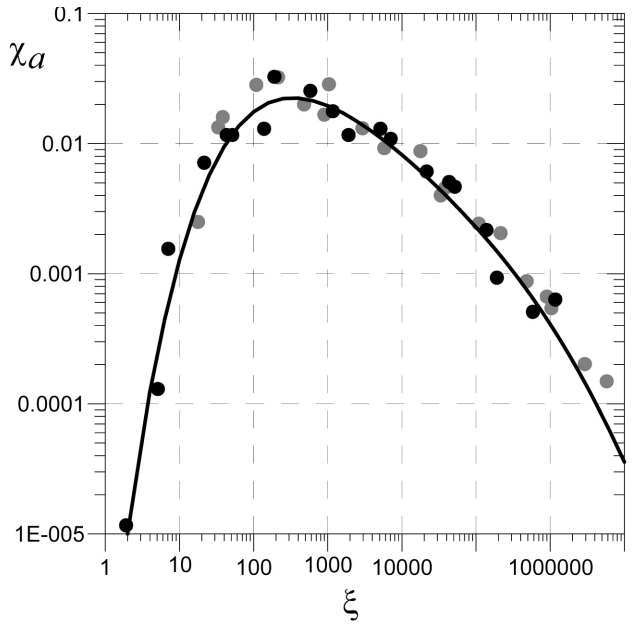

Fig. 3. Dimensionless atmospheric escape mass χ_a versus dimensionless erosional power ξ. Black circles show data for escape velocity of 11.2 km/s, gray circles show data for escape velocity of 5 km/s. Both data sets can be approximated by the curve (5) shown by black line.

drag. One more reason for more efficient atmospheric erosion by oblique impacts is that in oblique impacts a greater part of impact energy is released into the atmosphere (not into the solid target).

Figure 2 shows some typical escape regions, i.e., initial positions of escaping air. The escape region for the vertical impact of an asteroid 1 km in diameter looks like a cylinder, only the air surrounding the wake is accelerated to high altitudes. Escape regions for oblique impacts and for impacts of very large (>10 km) projectiles look like cones. It should be noted that the air initially situated along the trajectory at a distance of a few projectile diameters from the Earth's surface is usually not accelerated to high velocities. Just before the projectile strikes the ground surface, this air is trapped in the shock-compressed layer in front of the projectile. After the impact, a part of this air is forced into the target, mixes with melt, and is later ejected with relatively low velocity. The other part spreads along the surface outside the wake (and outside the plume). This effect has been considered in more details in Shuvalov and Artemieva (2002). It is more apparent for the impacts of large (>10 km) projectiles.

Numerical simulations show that the most efficient (from the viewpoint of atmospheric erosion) angle lies within the range from 30° to 45° for the smallest (1 km) projectiles under consideration and decreases to 15° for large projectiles 10 and 30 km in diameter.

Atmospheric erosion induced by the impacts of smaller (100 to 1000 m) projectiles is not considered in this paper. However, Nemtchinov and Shuvalov (2003) and Svetsov (2007) have shown that in such impacts air escapes only through the wake. Thus, it is reasonable to suppose that vertical impacts of such projectiles erode the atmosphere more efficiently than oblique ones, because in oblique impacts "the explosion" occurs outside the wake (see Fig. 1). As a result, it can be concluded that the most efficient angle (from the viewpoint of high atmospheric erosion) decreases when projectile size increases.

The blowoff model (Vickery and Melosh 1990) estimates the amount of air escaping the Earth after a Chicxulub-like impact (5×10^{30} erg, 9 km-radius asteroid of 10^{19} g) as 7×10^{16} g (0.7% of the projectile mass). The amount of escaping projectile material is about 25%. Newman et al. (1999) estimated the total amount of escaping gas (air and projectile vapor), expressed as a function of the initial projectile mass), as 4 to 7%. In the present simulations the values depend on impact angle. The escaping air mass equals 6, 1, 0.5, 0.2, and 0.05% for impact angles 15, 30, 45, 60, and 90° (vertical) correspondingly. The escaping projectile amount equals 30, 30, 4, 0.4, and 0.05% for the same angles. Note that even the simple estimates correlate better with angle averaged values than the results of numerical modeling of vertical impacts.

The impact process, the evolution of impact plume, and, consequently, atmospheric erosion strongly depend on impact "efficiency." The "efficiency" depends on projectile size, projectile density, impact velocity, etc. In this paper the erosional efficiency or erosional power is characterized by a dimensionless variable ξ, defined as

$$\xi = \frac{D^3 \rho_{pr} (V^2 - u_{esc}^2)}{H^3 \rho_0 \quad u_{esc}^2 (\rho_t + \rho_{pr})}, \tag{2}$$

where ρ_{pr} and ρ_t are densities of projectile and target materials, ρ_0 is air density at the surface, H is the atmospheric scale height, and V is impact velocity.

Figure 3 summarizes all the data on atmospheric erosion presented in Table 1 and Table 2 in the form of a dependence of normalized angle-averaged escaping air mass χ_a on the value of dimensionless erosional power ξ. The angle-averaged value of the escaping mass m (for both air, projectile, and target materials) was determined from summation over impact angles α_i = 15, 30, 45, 60, and 90 degrees:

$$m = \sum_i m_i \psi_i . \tag{3}$$

Here m_i is the escaping mass for impact angle α_i,

$$\psi_i = \int_{\alpha_{i-1/2}}^{\alpha_{i+1/2}} \sin(2\alpha) d\alpha$$

is the probability of impact at this angle. The normalized atmospheric mass χ_a is defined as

$$\chi_a = \frac{m_a}{M} \frac{u_{esc}^2}{(V^2 - u_{esc}^2)}, \tag{4}$$

where M is initial projectile mass. One can see that all the data

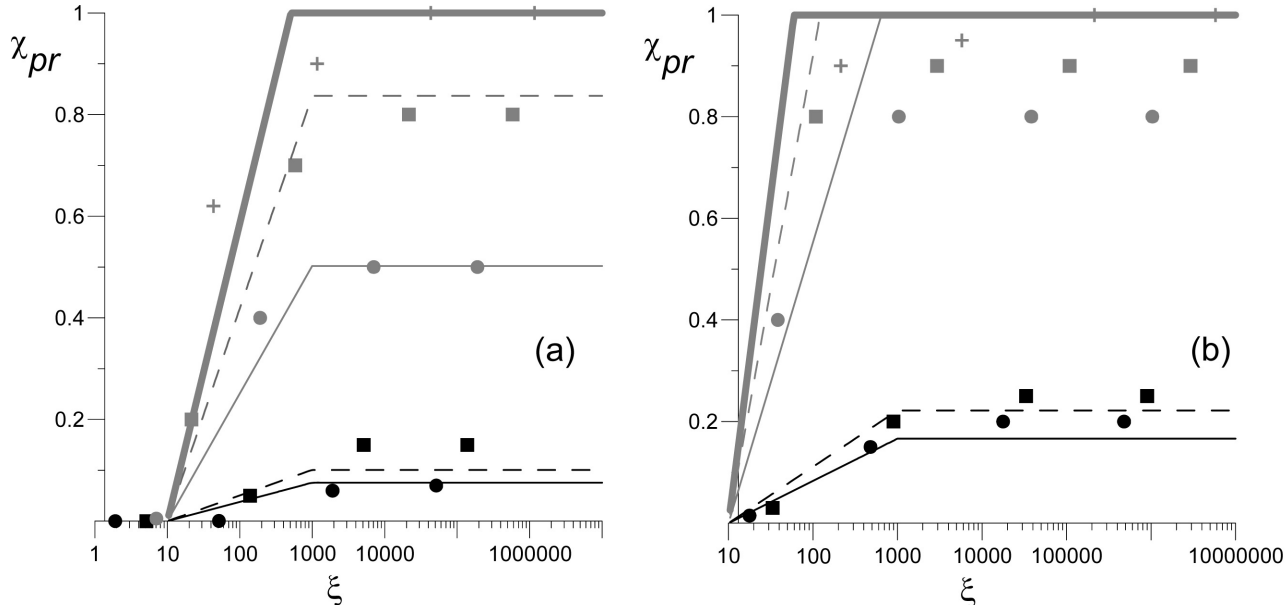

Fig. 4. Dimensionless mass of escaping projectile material χ_{pr} versus dimensionless erosional power ξ. Black circles show data for asteroids with $V = 15$ km/s, black squares show data for asteroids with $V = 20$ km/s, gray circles show data for comets with $V = 30$ km/s, gray squares show data for comets with $V = 50$ km/s, gray crosses show data for comets with $V = 70$ km/s. Plate (a) shows data for escape velocity 11.2 km/s, plate (b) shows data for escape velocity 5 km/s. The data can be approximated by simple curves (6). Solid and dashed black lines show approximations for asteroid impacts at 15 and 20 km/s correspondingly, thin solid, dashed and thick gray lines show approximations for cometary impacts at 30, 50, and 70 km/s correspondingly.

can be approximated by one polynomial curve if the variables ξ and χ_a are used:

$$\lg\chi_a = 6.375 + 5.239(\lg\xi) + -2.121(\lg\xi)^2 + 0.397(\lg\xi)^3 - 0.037(\lg\xi)^4 + 0.0013(\lg\xi)^5 . \quad (5)$$

The curve has a maximum at $\xi = 400$. Atmospheric erosion is negligible at small ξ because the impact plume is small, strongly decelerates in the atmosphere, and can not accelerate large atmospheric mass to high velocities. At high ξ real atmospheric erosion continues to grow (although very slowly), but the relative escaping mass χ_a decreases because the real escaping mass m_a is restricted by the total atmospheric mass. Atmospheric erosion induced by asteroid impacts is not large, the escaping atmospheric mass does not exceed a few percent of impactor mass. The maximum ratio of m_a/M (up to 0.15) is reached in very oblique (15° to 30° to horizon) impacts of asteroids 3 to 10 km in diameter. Cometary impacts are more efficient, and the escaping air mass can reach up to a few tens percent. In both cases, projectiles 3 km in diameter are the most efficient for high atmospheric erosion.

The data for escape velocity of 5 km/s are also presented in Tables 1–2 and in Fig. 3. They also can be approximated by the same polynomial curve described by Equation 5. These data can be used for estimates of impact induced atmospheric erosion on Mars (when and if it had an atmosphere of the same density and the same stratification as the modern Earth's atmosphere). In this case atmospheric erosion is much stronger.

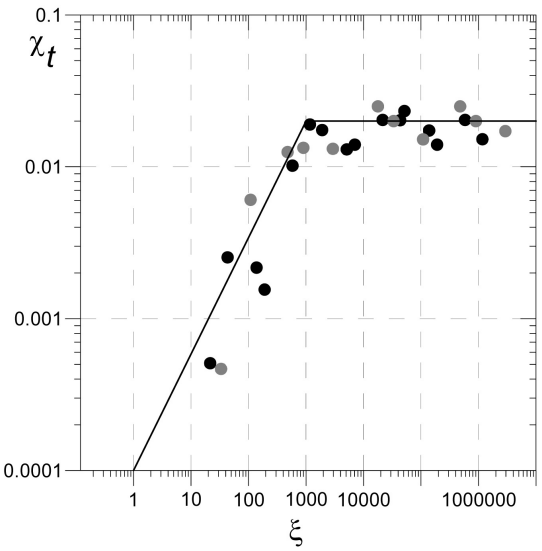

Fig. 5. Dimensionless mass of escaping target material χ_t versus dimensionless erosional power ξ. Black circles show data for escape velocity 11 km/s, gray circles show data for escape velocity 5 km/s. The data can be approximated by the curve (7) (black line).

Figure 4 shows the dependence of relative escaping projectile mass (also angle-averaged) $\chi_{pr} = \frac{m_{pr}}{M}$ on the same dimensionless erosional power ξ. These data can also be approximated by one simple formula:

$$\chi_{pr} = \min\{1, 0.07(\rho_t/\rho_{pr})(V/u_{esc})(\lg\xi - 1)\}. \quad (6)$$

Table 3. Relative masses of escaping air, projectile and target material for different variants of cometary (marked by*) and asteroidal impacts D-V-A (D-projectile diameter (in km), V-impact velocity (km/s), A-impact angle), two values of escape velocity (11.2 and 5 km/s), and atmospheres of different density. δ is a relative atmospheric density (with respect to the current Earth's atmosphere). Angle-averaged escaping masses are shown in brackets in lines for 45 degree impact angles. The values of dimensionless erosional power for escape velocities 11.2 km/s ($\xi_{11.2}$) and 5 km/s (ξ_5) are given in the last column.

Variant	δ	m_a/M (u_{esc} = 11.2)	m_a/M (u_{esc} = 5)	m_{pr}/M (u_{esc} = 11.2)	m_{pr}/M (u_{esc} = 5)	m_t/M (u_{esc} = 11.2)	m_t/M (u_{esc} = 5)	$\xi_{11.2}$ (ξ_5)
10-20-15	10	0.1	0.7	0.5	0.9	0.002	0.04	
10-20-30	10	0.06	0.2	0.2	0.6	0.05	0.4	
10-20-45	10	0.025 (0.034)	0.1 (0.17)	0.06 (0.11)	0.2 (0.3)	0.02 (0.018)	0.4 (0.28)	5.1e2 (3.3e3)
10-20-60	10	0.005	0.05	0	0.1	0	0.2	
10-20-90	10	6e-4	0.01	0	2e-3			
3-50-15*	10	0.2	9	0.03	0.9	0	0.2	
3-50-30*	10	0.5	6	0.25	0.6	0.08	0.7	
3-50-45*	10	0.4 (0.31)	4 (4.4)	0.3 (0.24)	0.9 (0.87)	0.07 (0.042)	1 (0.97)	58 (2.9e2)
3-50-60*	10	0.15	2.5	0.2	1	5e-3	1.5	
3-50-90*	10	0.1	1	0.4	1	0	1	
1-20-15	0.1	2e-3	1	0	0.2	0	0.007	
1-20-30	0.1	0.05	0.04	0.025	0.5	4e-4	0.3	
1-20-45	0.1	0.015(0.015)	0.2 (0.21)	3e-3 (0.01)	0.2 (0.21)	5e-5 (0.00015)	0.3 (0.21)	51 (3.3e2)
1-20-60	0.1	1e-4	0.06	0	0.05	0	0.15	
1-20-90	0.1	1e-5	0.005	0	0.01	0	0.005	
3-20-15	0.1	0.2	0.4	0.5	0.8	0.02	0.09	
3-20-30	0.1	0.05	0.1	0.3	0.6	0.05	0.5	
3-20-45	0.1	0.015 (0.04)	0.03 (0.084)	0.06 (0.14)	0.25 (0.3)	0.04 (0.022)	0.4 (0.31)	1.4e3 (9e3)
3-20-60	0.1	0.004	0.015	0.007	0.06	0.001	0.2	
3-20-90	0.1	2e-4	0.03	1e-4	0.01	2e-4	0.02	
1-50-15*	0.1	1.5	6	0.3	0.7	0.01	0.25	
1-50-30*	0.1	0.9	3	0.7	0.9	0.04	1	
1-50-45*	0.1	0.5 (0.62)	1.5 (2.1)	0.8 (0.6)	1 (0.9)	0.2 (0.18)	2 (1.5)	2.2e2 (1.1e3)
1-50-60*	0.1	0.3	0.8	0.6	1	0.2	2	
1-50-90*	0.1	0.05	0.6	0.6	1	0.08	2	
3-50-15*	0.1	0.5	2	0.8	1	0.02	0.3	
3-50-30*	0.1	0.3	0.9	0.6	1	0.1	0.7	
3-50-45*	0.1	0.2 (0.22)	0.3 (0.68)	0.9 (0.7)	1 (0.97)	0.4 (0.23)	2 (1.53)	5.8e3 (2.9e4)
3-50-60*	0.1	0.1	0.5	0.3	0.9	0.2	2	
3-50-90*	0.1	0.01	0.3	0.5	1	0.2	2	
10-20-15	100	8e-4	1	0	0.3	0	3e-5	
10-20-30	100	0.02	0.8	0	0.6	0	0.1	
10-20-45	100	0.02 (0.012)	0.3 (0.43)	0 (0)	0.3 (0.28)	0 (0)	0.2 (0.1)	51 (3.3e2)
10-20-60	100	5e-3	0.15	0	0.05	0	0.03	
10-20-90	100	0.004	0.06	0	0.001	0	0	
10-50-15*	100	1	5	0.2	0.6	0	0.006	
10-50-30*	100	0.9	4	0.4	0.9	0.07	0.5	
10-50-45*	100	0.6 (0.6)	3 3	0.3 (0.3)	0.8 (0.76)	0.06 (0.1)	1 (0.74)	2.2e2 (1.1e3)
10-50-60*	100	0.3	2	0.3	0.7	0.1	1	
10-50-90*	100	0.2	0.4	0.3	0.6	0.2	0.4	

No projectile material escapes at $\xi < 10$. At $\xi > 10$ the value of χ_{pr} linearly increases (in logarithmic scale) until it reaches the airless limit (when atmospheric drag is negligible for plume expansion). Note that only a small part of asteroidal material (<10–20%) escapes after the impact, whereas most of the cometary material escapes the Earth if the comet is large enough ($\xi > 1000$). Decrease of escape velocity down to 5 km/s strongly increases the portion of escaping projectile material.

The data on the solid target escaping mass (see Fig. 5) can also be approximated by a simple equation:

$$\lg\chi_t = \min\{0.02, -4 + 1.15\lg\xi\}, \quad (7)$$

where

$$\chi_t = \frac{m_t}{M}\frac{u_{esc}^2}{(V^2 - u_{esc}^2)}. \quad (8)$$

Table 4. Calculated and approximated values of dimensionless mass of escaping projectile material for the variants with rarefied and dense atmospheres listed in Table 3.

			$\chi_{pr}(u_{esc} = 11.2)$			$\xi_{pr}(u_{esc} = 5)$	
Variant	δ	$\xi_{11.2}$	Calc.	Eq (6)	ξ_5	Calc.	Eq (6)
10–20	10	5.1e2	0.1	8.6e-2	3.3e3	0.3	0.22
3–50*	10	58	0.24	0.32	2.9e2	0.87	1
1–20	0.1	51	2e-2	3.6e-2	3.3e2	0.21	0.17
3–20	0.1	1.4e3	0.14	0.10	9.0e3	0.30	0.22
1–50*	0.1	2.2e2	0.60	0.56	1.1e3	0.90	1
3–50*	0.1	5.8e3	0.70	0.84	2.9e4	0.97	1
10–20	100	51	0	3.6e-2	3.3e2	0.28	0.17
10–50*	100	2.2e2	0.30	0.56	1.1e3	0.76	1

Up to 0.07 M of the solid Earth material (granite) can be accelerated above escape velocity (11.2 km/s) after large asteroidal impacts and up to 0.5 M of the solid Earth can escape after large cometary impacts. The ejected target mass increases to 0.6 M and 7 M, respectively, when escape velocity decreases to 5 km/s.

All asteroid impacts under consideration result in increase of the total Earth's mass ($m_a + m_{pr} + m_t < M$), whereas large cometary impacts (with V = 50 km/s and 70 km/s) result in decrease of the total Earth's mass ($m_a + m_{pr} + m_t > M$).

In order to follow the possible evolution of the Earth's atmosphere one needs to estimate atmospheric erosion for different atmospheric densities (not only for the current Earth's atmosphere). Some numerical simulations were performed for cometary and asteroidal impacts against the Earth covered by rarefied (density smaller than the current by a factor of 10) and more dense (by a factor of 10 and 100) atmospheres. Density stratification (i.e., distribution of relative density) was the same in all the simulations. The results are presented in Tables 3, 4 and in Figs. 6, 7. One can see that the results can also be satisfactory approximated (within a factor of two) by relations (5–7).

The most effective projectile size (from the viewpoint of atmospheric erosion) strongly depends on atmospheric density and changes from 1–3 km for a 10 times rarefied atmosphere to about 10–30 km for a very dense (with density increased by a factor of 100) atmosphere. The most effective size corresponds to $\xi = 400$.

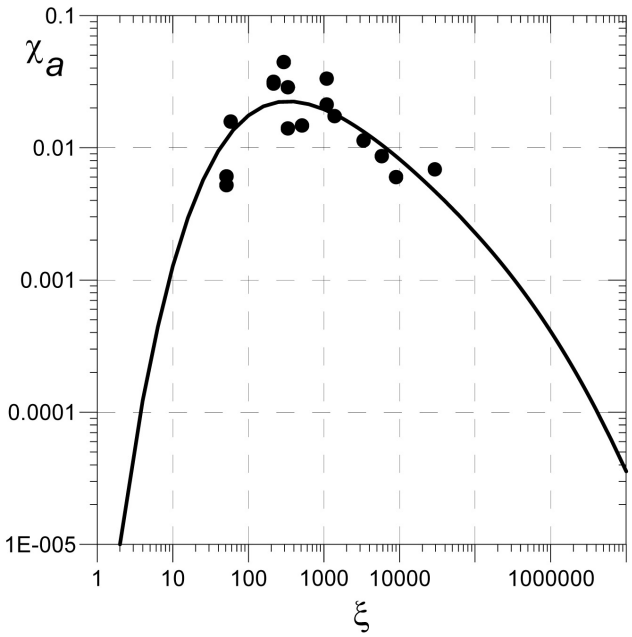

Fig. 6. Dimensionless atmospheric escape mass χ_a versus dimensionless erosional power ξ for the variants with rarefied and dense atmospheres listed in Table 3. The data can be approximated by the same (as in Fig. 3) curve (5) shown by black line.

CONCLUSIONS

The numerical simulations described above clearly demonstrate the strong influence of impact angle on atmospheric erosion induced by impacts. In most cases under consideration and, in particular, in all impacts providing the maximum erosion (at fixed projectile size and impact velocity) vertical impacts produce considerably smaller escaping air mass than oblique ones. The small erosion in a vertical impact is related to the influence of a wake. In vertical impacts an impact plume expands preferably within the rarefied wake and accelerates a smaller mass of atmospheric air.

The most efficient impact angle depends on a projectile size. It equals 30° to 45° for projectiles 1 km in diameter ($\xi << 400$) and decreases to 15° for large projectiles 10 and 30 km in diameter ($\xi \geq 400$). In general, high velocity comets produce stronger atmospheric erosion than asteroids impacting the Earth with lower velocities.

Over the wide range of considered impact parameters (projectile sizes from 1 to 30 km, impact velocities from 15 to 70 km/s, escape velocities from 5 to 11.2 km/s, projectile densities from 1 to 3.3 g/cm^3, normal atmospheric densities varying by three orders of magnitude), the angle averaged escaping mass can be approximated by a simple polynomial function of dimensionless erosional power ξ. A deviation of calculated numbers from the polynomial approximation (5) does not exceed a factor of 2, in most cases the deviation is smaller. Such accuracy seems to be reasonable for current models of the evolution of planetary atmospheres. It also

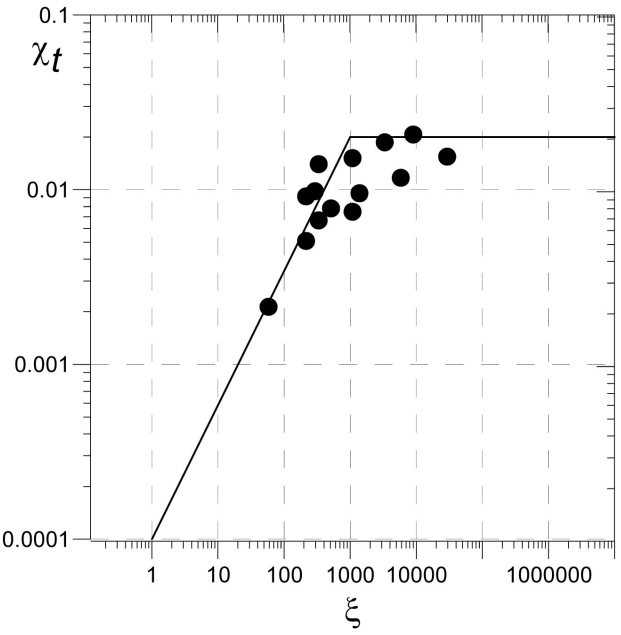

Fig. 7. Dimensionless mass of escaping target material χ_t versus dimensionless erosional power ξ for the variants with rarefied and dense atmospheres listed in Table 3. The data can be approximated by the same (as in Fig. 5) curve (7) shown by black line.

correlates with the accuracy of numerical results themselves, taking into account the hydrocode accuracy, possible variations in projectile shape and structure, variations of target structure, variations of atmospheric stratification, etc. The data for escaping projectile and target material can be also approximated by simple analytical functions with similar accuracy. However, it should be noted that the approximations (5–7) may not be valid at small impact velocities (below 10–15 km/s) in the absence of a well-developed vapor plume.

In terms of atmospheric erosion, the most efficient projectile size depends on atmospheric density and increases as the density increases.

Approximation (5) supplemented with the projectile flux permits the calculation of atmospheric losses during a certain time period. While the impactor flux and its variations with time are approximately known (Neukum et al. 2001), the comet fraction in this flux is still under discussion. Assuming that the flux is exclusively asteroidal, one can estimate that modern Earth loses 0.05% of its atmosphere (due to impact erosion) over a 1 Gyr period. An occurrence of comets would increase this value, but the loss remains negligible. However, the impact-induced erosion of the Earth's atmosphere could be important (i.e., comparable with the total atmospheric mass) in the period of the Late Heavy Bombardment and earlier.

In closing, it should be noted that a considerable part (more than a half for the modern Earth) of impactors fall into the ocean. The presence of a water layer can substantially change the parameters of the impact plume and, consequently, change the mass of escaping air. The results probably depend on the ratio of projectile size to water depth. However, this is a subject for another study.

Acknowledgments–The author thanks V. Svetsov for fruitful discussions, J. Melosh and W. Newman for valuable reviews, and editor N. Artemieva for the help with this paper.

Editorial Handling—Dr. Natalia Artemieva

REFERENCES

Cameron A. G. W. 1983. Origin of the atmospheres of the terrestrial planets. *Icarus* 56(2):195–201.

Chyba C. F. 1990. Impact delivery and erosion of planetary oceans in the early inner solar system. *Nature* 343:129–133.

Kompaneets A. S. 1960. A point explosion in an inhomogeneous atmosphere. *Soviet Physics Doklads English Translation* 5:46–48.

Kosarev I. B. 2008. Optical characteristics and equations of state of invading the Earth's atmosphere cosmic body material vapors (abstract). International Conference "100 years since Tunguska phenomenon: Past, present and future". Moscow: IDG RAS. pp. 128–129.

Kuzmitcheva M. and Ivanov B. 2008. Cometary hazards. In *Catastrophic events caused by cosmic objects*, edited by Adushkin V. V. and Nemchinov I. V. Berlin: Springer-Verlag. pp. 117–130.

Nemchinov I. V. and Shuvalov V. V. 2003. Geophysical consequences of impacts of small asteroids and comets. In *Geofizicheskie protsessy v nizhnikh i verkhnikh obolochkakh Zemli* (*Geophysical processes in upper and lower shells of the Earth)*. Moscow: IDG RAN. pp. 36–47.

Neukum G., Ivanov B. A., and Hartmann W. K. 2001. Cratering records in the inner solar system in relation to the lunar reference system. *Space Science Review* 96:55–86.

Newman W. I., Symbalisty E. M. D., Ahrens T. J., and Jones E. M. 1999. Impact erosion of planetary atmospheres: Some surprising results. *Icarus* 138:224–240.

Pierazzo E., Vickery A. M., and Melosh H. J. 1997. A reevaluation of impact melt production. *Icarus* 127:408–423.

Pierazzo E., Kring D. A., and Melosh H. J. 1998. Hydrocode simulation of the Chixulub impact event and the production of climatically active gases. *Journal of Geophysical Research* 103(E12):28607–28626.

Shuvalov V. V. 1999. Multi-dimensional hydrodynamic code SOVA for interfacial flows: Application to thermal layer effect. *Shock Waves* 9(6):381–390.

Shuvalov V. V. and Artemieva N. A. 2000. Atmospheric erosion and radiation impulse induced by impacts. In *Catastrophic events and mass extinctions: Impacts and beyond*. LPI Contribution 1053. Houston: Lunar and Planetary Institute. pp. 199–200.

Shuvalov V. V. and Artemieva N. A. 2002. Atmospheric erosion and radiation impulse induced by impacts. In *Catastrophic events and mass extinctions: Impacts and beyond*, edited by Koeberl C. and MacLeod K. G. GSA Special Paper 356. Boulder: Geological Society of America. pp. 695–704.

Svetsov V. V. 1996. Total ablation of the debris from the 1908 Tunguska explosion. *Nature* 383:697–699.

Svetsov V. V. 2007. Atmospheric erosion and replenishment induced by impacts of cosmic bodies upon the Earth and Mars. *Solar System Research* 41(1):28–41.

Thompson S. L. and Lauson H .S. 1972. *Improvements in the Chart*

D radiation-hydrodynamic CODE III: Revised analytic equations of state. Report SC-RR-71 0714. Albuquerque: Sandia National Laboratory. 119 p.

Vickery A. M. 1994. Impact erosion of atmospheres (abstract). 25th Lunar and Planetary Science Conference. pp. 1437–1438.

Vickery A. M. and Melosh H. J. 1990. Atmospheric erosion and impactor retention in large impacts with application to mass extinctions. In *Global catastrophes in Earth history,* edited by Sharpton V. L. and Ward P. D. GSA Special Paper 247. Boulder: Geological Society of America. pp. 289–300.

Zahnle K., Pollack J. B., and Kasting J. F. 1990. Mass fractionation of noble gases in diffusion-limitic hydrodynamic hydrogen escape. *Icarus* 84:503–527.

Zahnle K., Pollack J. B., and Gripspoon D. 1992. Impact-generated atmospheres over Titan, Ganymede, and Callisto. *Icarus* 95:1–23.

Zel'dovich Ya. B. and Raizer Yu. P. 1967. *Physics of shock waves and high-temperature hydrodynamic phenomena.* New York: Academic Press. 916 p.